

ARTICLE



Numerical investigation of switching features of a hydraulic seat valve with annular flow geometry

Niels Christian Bender ^a, Henrik Clemmensen Pedersen ^a, Bernd Winkler^b and Andreas Plöckinger^b

^aDepartment of Energy Technology, Aalborg University, Aalborg, Denmark; ^bLinz Center of Mechatronics, GmbH, University, Linz, Austria

ABSTRACT

This article presents a numerical framework for investigating transient features of hydraulic valves, specifically poppet type designs suited for digital hydraulics. The objective is to determine the validity of the state-of-the-art lumped parameter models (LPM) of fluid dynamical phenomena during switching of such valves. Knowledge about analytically valid models for simple situations are used together with complex Computational Fluid Dynamics simulations, which is not a novel concept, but the procedure at which this is done is. The idea behind the research is to consider a numerical framework with dynamic capabilities as a sufficiently accurate representation of reality. Thereby, strategic simulation cases can be applied to understand the features of the design. The sought dependencies of the valve was revealed by conducting several ‘experiments’ through the simulation framework which allows analysis of practically difficult operating conditions. The results of the numerical framework reveals how and where the state-of-the-art LPM deviate (e.g. that fluid displaced by the plunger itself is not directly proportional to velocity, that fluid inertia is significant and that the fluid-induced force is non-linear with changes in velocity).

ARTICLE HISTORY

Received 9 February 2018
Accepted 19 June 2018

KEYWORDS

Digital hydraulics; hydraulic valves; computer aided analysis; design methodology

1. Introduction

Hydraulic seat valves are one of the main components used in the fluid power branch called digital hydraulics – for example, for Discrete Displacement cylinders (Huova *et al.* 2010, Hansen *et al.* 2013), Digital Displacement pumps/motors (Ehsan *et al.* 2000) or hydraulic buck converters (Kogler *et al.* 2010). In this regard, several different types of fast-switching on/off valves have been proposed both commercially and custom-made designs evolving from research projects (Uusitalo *et al.* 2010, Winkler *et al.* 2010, Wilfong *et al.* 2011, Roemer *et al.* 2015a, Noergaard 2017). Specifically, Wilfong *et al.* 2011, Roemer *et al.* 2015a, Noergaard 2017 have their designs made exclusively for application in Digital Displacement Units (DDU). This means high flow rates with preferably low throttling losses. The primary focus is concerned with the overall switching performance, and optimisation of this is done in various ways. The fluid dynamics receives a mixed amount of attention in the reviewed design frameworks, and especially Lumped Parameter Models (LPM) of the transient effects receives limited attention.

Digital valves are intended to switch several billion times through their lifetime, and this imposes concerns about durability. One factor that comes into consideration is the deceleration profile of the moving member when it nears the valve seat (Lewis 2007). Therefore, it is of interest to include accurate fluid dynamics in design

frameworks. Furthermore, a simplification of the chosen modelling framework when doing optimisation may potentially lead to inaccurate optimums.

The purpose of this article is to investigate the significant fluid dynamical properties of an annular seat valve designed for DDU and compare to the state of the art.

1.1. Simulation of seat valves – state of the art

Various types of modelling frameworks for FSVs have been proposed in the literature, the required modelling effort will vary from application to application, but in any design framework it is valuable to understand the consequences of ones limitations. In short, the modelling accuracy can enhance knowledge about a systems bandwidth and about the durability of one design compared to another. A general structure of a design framework is proposed in (Bender *et al.* 2017b), along with a broad review of state-of-the-art design frameworks with relation to the mechanical topology of hydraulic valves. This work focuses on three phenomena: movement-induced forces and flows as well as pressure-driven flow.

1.2. Movement-induced flow

Whenever a solid body is moving through a medium, that medium is dislocated which results in flows. The

state-of-the-art approach to deal with this phenomenon when modelling switching valves for DDU is to use the valve's plunger shadow area and multiply it with its velocity (Roemer *et al.* 2013, Noergaard 2017). This area can for annular poppet geometries become significant. A similar consideration is taken by (Knutson and Van De Ven 2016), where the dynamics of a check valve is analysed. The flow through the valve is estimated from the orifice equation plus a term proportional to the velocity of the moving part and the shadow area of the valve (the movement-induced flow).

Among the early work (Ehsan *et al.* 2000), this phenomena was not considered.

The actual occurrence of this phenomenon will govern the forces acting on the plunger in the switching instant (i.e. influencing machine efficiency and switching speeds). A design that facilitates this optimally will only be located if it is modelled accurately, and is therefore relevant to investigate to improve the mechanical topology.

1.3. Movement-induced force

Movement of solid bodies in viscous fluids means resisting drag forces and additional mass from the fluid displaced by the moving body. Focusing on these forces several propositions have been made to apply Computational Fluid Dynamics (CFD) frameworks and thereby estimate a LPM (Roemer *et al.* 2013, 2015b, Noergaard *et al.* 2015, Bender *et al.* 2017a), which are then included in design frameworks to optimise the valve. Some of the LPMs relies on transient numerical simulation to determine fluid parameters, others estimates a constant value based on the geometry. None of the models enjoys universal application in the entire operating range. Specifically, an accurate expression of the drag force is missing and how it relates to the valves lift.

The literature contains several examples of analytic solutions to fluid drag on spheres, discs and other simple geometries when moving in an unbounded fluid domain, (e.g. Lai and Mockros 1972, Lai 1973). Also, the topic of fluid displaced by a given geometry has been addressed, and shown to be proportional to the added mass (Brennen 1982). However, when the fluid domain is bounded and the geometry takes complicated shapes, a general solution is not easily obtained. As an alternative, a Reynolds Averaged Navier Stoke's (RANS) formulation can be solved numerically by CFD. This methodology is well proven, and is therefore proposed to aid in identifying transient phenomena related to the fluid dynamics of annular seat valves.

1.4. Pressure-driven flow

The governing equations of flow through hydraulic valves in DDU typically apply quasi-steady lumped

fluid models (Roemer *et al.* 2014). A flow is therefore an instantaneous consequence of an instantaneous pressure difference and vice versa. Therefore, the force related to this flow is also instantaneous. The LPM presented in (Roemer *et al.* 2013) is applied in the context of a DDU and the results are compared with a 3D CFD formulation. The main deviation between the models occur during the switching phase of the valves, where the transient pressure is observed to oscillate more for the CFD simulation compared with the LPM. These oscillations are comparable with measurements on a DDU (Noergaard *et al.* 2017) leading to the hypothesis that the suggested LPM discards some of the transient term(s).

The transient behaviour of flow through an orifice deviated from the response predicted by a quasi-steady analysis when a constant pressure difference was applied (Funk *et al.* 1972). A solution strategy including fluid inertia was suggested and this showed better agreement with experimental data. A similar strategy is applied in this study.

The main hypothesis of this study is that it is possible to check the validity of state-of-the-art LPM during the switching event of seat valves, by application of a CFD modelling framework.

This leads to conclusions that: (a) fluid displaced by the moving plunger is non-linearly depending upon the plunger lift and velocity, (b) the force induced by the fluid on the moving member is highly non-linear and (c) a fluid inductance is observed from CFD and accurately described by an approximated analytical expression.

1.5. Structure of the paper

Initially the broad perspective is given by presenting a DDU developed in the HyDrive project and clarifying the geometric topology of the hydraulic valve that is of interest. A numerical framework is applied to analyse the valve since it facilitates user-defined simulation environments. This CFD procedure is elaborated in the text. Different simulation cases are proposed in order to achieve useful information about the valve. The results hereof are used to illustrate different valve features, which are compared to existing LPMs. This is used to propose novel LPMs and to conclude where simplifications are necessary. Finally, the main conclusions and outlook for further work are presented.

2. Presentation of the system

The overall mechatronic system that is the primary application of the hydraulic valve analysed in this research is a DDU. These machines belong to the field of fluid power machines. The flow to and from

the radially located pistons in the machine are controlled by switching valves, which are respectively connected to a high- and low- pressure manifold. This allows generation of shaft torque or a pressurised flow depending on the switching constellation.

The valve topology that is the basis for this analysis is an active check valve (ACV) as originally presented in (Noergaard *et al.* 2016). This has been optimised for low power losses, by minimising the pressure loss while maintaining the required flow rate. The system is decomposed to the two essential parts for this analysis, the valve plunger and the valve seat as shown in Figure 1.

The figure shows a cropped view of the valve plunger and seat with positive flow following in the direction of the arrows. The simplification from three-dimensional (3D) to 2D shows locations of the zones described in Table 1. White areas in the 2D part of Figure 1 are respectively seat and plunger.

The applied actuation technology is a moving voice-coil, which means that a force can be generated rapidly, with magnitude (60–80 N) sufficient to close the valve in less than 2 ms (moving mass is around 19 g). Boundary conditions are enforced on the walls and on Line 1 & 2 and the relevant parameters of the valve are shown on Figure 1.

The presented simplification is constructed to encapsulate some of the asymmetries (e.g. the flow venting paths of the plunger will be a cause of asymmetric flow conditions). These play a role in calculating the hydrodynamic damping, and may thus be a source of error. However, this is not considered a major issue compared with the enclosed decrease in computational effort.

Table 1. Mesh zone definitions and parameters.

Parameter	Mesh technique and settings
Zone 1 and 5	Stationary unstructured boundary zones
Zone 2 (biased) and 4	Dynamic quadrilaterals re-meshing and layering zones
Zone 3 and 6	Rigid body unstructured quadrilateral-dominated mesh zones
Length of the edge and elements ($L_{element}$)	$l_s, 3e-2$ mm
Number of elements (n)	$round\left(\frac{L}{l_{element}}\right) = 83$
Bias factor (r)	20
Computed S_s and S_e	4.76e-3 and 9.52e-2 mm
# cells (coarse to fine)	1.9e4, 2.2e4, 3.6e4, 7.5e4
Cell collapse and split (a_c, a_s)	0.3/0.4

3. Definition of the numerical framework

The overall modelling framework is based on the one presented in (Bender *et al.* 2017b), but in this article an elaboration of the framework's functionality is given. The CFD software package Fluent 17.2 is used to carry out the computations. The flow chart presented in Figure 2 illustrates how the software is structured.

The solver algorithm is based on the Finite Volume Method (FVM) and has been designed to solve convection-diffusion equations by discretisation and linearisation techniques. This can then be solved for pressure, momentum, energy etc.

3.1. Spatial discretisation and refinement

The numerical solution to most problems is strongly influenced by the meshing technique (used to discretise a complex geometry into simple pieces). The analysis presented is intended to reveal flow phenomena under ideal and simple conditions, which is why

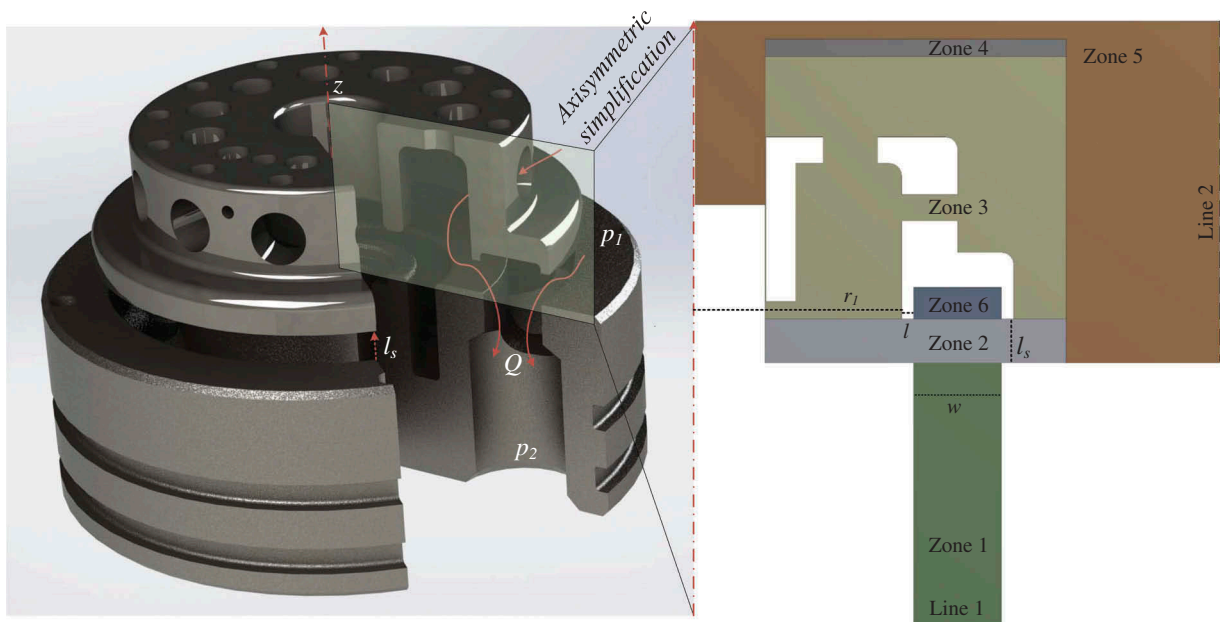


Figure 1. Left: mechanical topology of active check valve (ACV). Right: An axisymmetric simplification used in CFD simulation.

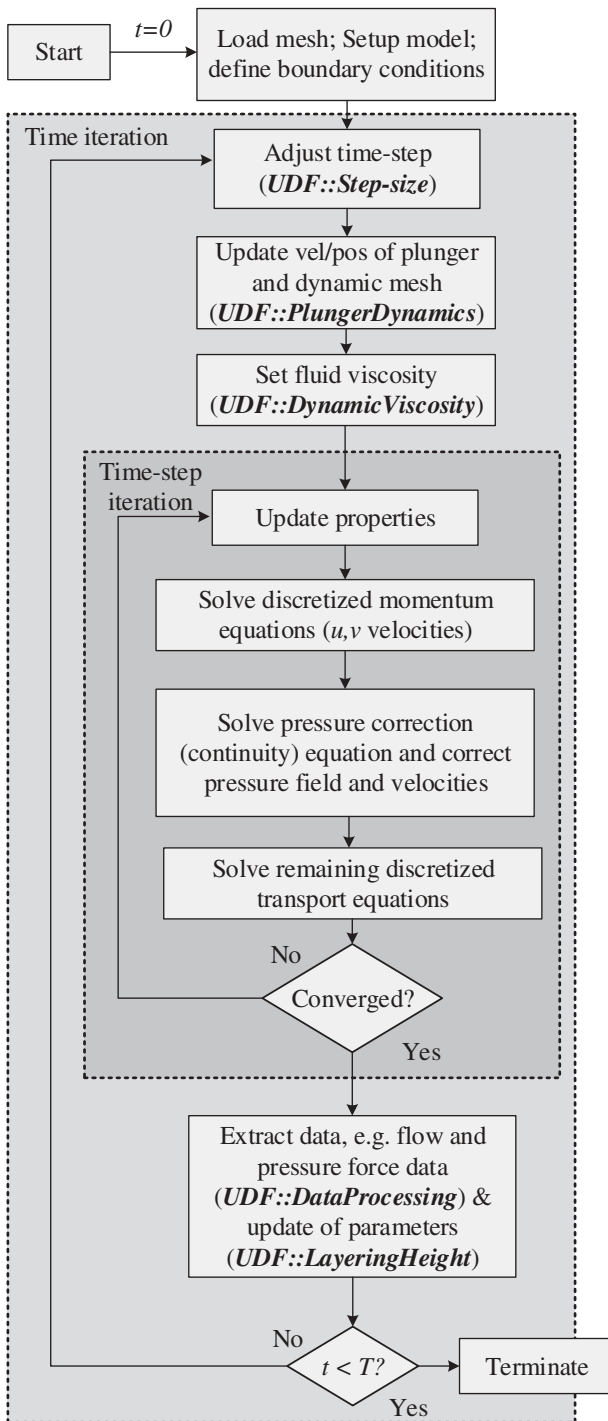


Figure 2. Transient CFD algorithm with user-defined modification. The analysis is initialised with initial conditions. Hereafter, post-processed data from each converged time-step is used to update the step-size thresholds and movement of the plunger. Then the viscosity in the fluid domain is calculated (depends on pressure and temperature). A pressure-based solver algorithm (SIMPLE (Malalasekera and Versteeg 2006)) gives the solution and data is extracted to a separate file.

a 2D axisymmetric approximation is chosen. This is justified by the symmetric nature of the valve resulting in a decrease of computational cost. However, this comes with the drawback that any symmetry breaking phenomena cannot be included.

The analysis requires a dynamic mesh since a solid body moves through a fluid. This is achieved by dividing the fluid domain into several zones with different properties as shown in Figure 1 and explanation in Table 1. The collapse of mesh cells are done by the layering technique, which requires a structured mesh (meaning only quadrilateral elements are allowed for 2D problems). Furthermore, Zone 2 is designed with a biased mesh that gets finer when approaching the seat in order to ensure a converging solution during switching. To maintain the simplicity of the analysis the plunger is assumed rigid, which is a fair approximation considering the deformations of the plunger relative to the movement.

The bias mesh is based on information given about the geometries' edge length, the bias factor and the number of desired cells. The meshing algorithm calculates change in cell size between each cell and the size of start and end cell by:

$$L = \sum_{i=0}^{n-1} S_s k^i; \frac{S_e}{S_s} = r = k^{n-1} \quad (1)$$

where L is the length of the edge where a biased mesh is desired, n is the number of elements required, S_s & S_e is the length of start and end cell respectively, k is the cell-to-cell expansion and r is the bias factor. This is used to understand the maximum allowed step-size, as elaborated later.

The dynamic mesh is updated with the layering technique, which either collapses or splits a cell if one of the two constraints is violated:

$$h < a_c h_{id}; h > (1 + a_s) h_{id} \quad (2)$$

where the ideal height, h_{id} , at a specific solid boundary is user defined as well as the collapse and split factors, a_c and a_s respectively, can be tuned.

The ideal height in the mesh zone is handled by the User Defined Function (UDF), UDF::LayeringHeight. The importance of this height has been investigated and most robust results are achieved if the value is simply fixed at a magnitude which corresponds to the size of the original mesh, therefore: $h_{id} = S_e$. Alternatively, different algorithms may be implemented to change h_{id} as function of the plunger lift to allow a finer mesh when the plunger is near the valve seat. However, results of this caused divergence for some simulations and therefore not used.

3.2. Fluid viscosity, stiffness and density

The density and viscosity of the fluid will influence the forces exerted on the rigid body and the fluid flow. These fluid properties are dependent upon temperature and pressure. This becomes relevant when two surfaces approach one another with high velocities, where local pressure rise will influence fluid

viscosity. Therefore, the Barus equation has been implemented to the numerical solver. The squeeze gap pressure depends on the plunger velocity and this effect does result in significant viscosity changes, by factors in between 2 and 44. This viscosity change will result in higher gap pressures, and this will enhance the change in viscosity. The actual medium is compressible due to presence of air and hence the density and stiffness will not remain constant. The importance of this was addressed for the same system in (Bender *et al.* 2017a) showing the validity of using an incompressible medium when studying the fluid-induced forces. Therefore, the fluid is considered incompressible in the analysis, which decreases the required simulation time considerably.

3.3. Turbulence models and solver choices

A transient solver is used since transient phenomena is the topic of interest. The pressure and velocity fields are solved with the Semi-Implicit Method for Pressure Linked Equations-Consistent (SIMPLEC) algorithm since it has stable convergence for a wide range of flow regimes, and generally requires less memory than other solvers. The turbulent two-equation model: Shear Stress Transport (SST) $k - \omega$ with low Reynolds corrections is the state-of-the-art model and therefore applied.

The regular highlighted drawback of two-equation models is the decreased solution accuracy of flows containing large adverse pressure gradients (Bardina *et al.* 1997), since the Boussinesq-Eddy viscosity assumption becomes invalid. However, since the focus is on low pressure differentials, this inherently also means that the adverse pressure gradient will be relatively small. The important simulation settings are displayed in Table 2.

3.4. Valve dynamics

The movement of the plunger is described by the force equilibrium. An actuator, a spring and the pressure of the surrounding medium govern this movement.

The equations of motion are solved by the Euler Forward Method, which has shown to give stable solutions (i.e. the eigenvalues of the system lies within the unit circle centered at $(-1,0i)$ in the complex plane). The iterative process is:

$$\ddot{z}_i = (F_{act,i} + F_{f,i} + F_{S,i}) * \frac{1}{m} \quad (3)$$

$$\dot{z}_i = \dot{z}_i\tau + \dot{z}_{i-1} \quad (4)$$

$$z_i = \dot{z}_i\tau + z_{i-1} \quad (5)$$

where m and z are the mass and the position of the moving member respectively, τ is the variable time-

Table 2. CFD simulation parameters.

Parameter	Value/description
Temperature	40 °C
Medium (oil VG-46)	872 kg/m ³
Plunger mass	19 g
Spring stiffness and preload	2.2 N/mm and 31 N
Viscous fluid model	SST $k-\omega$ with low re-correction
Wall B.C.	No slip
Line 1 and 2 B.C.	Pressure outlet
Solver	SIMPLEC
cont, u, v, k, ω -convergence	1e-4
Discretisation of: $p/k, \omega$	PRESTO/2nd order upwind
Discretisation of: u, v	1 st order upwind
<i>User Defined Functions (UDF)</i>	
UDF::Data Processing	Extract results, e.g. flow and forces
UDF::DynamicViscosity	Describes viscosity of each cell
UDF::LayeringHeight	Can alter the ideal height of layering zone
UDF::Step-size	Describes the step-size thresholds
UDF::PlungerDynamics	Describes the plunger movement

step, F_{act}, F_f, F_s are the forces of; the actuator, fluid and spring respectively.

In Equation (3) the fluid force is obtained from the UDF::DataProcessing in Figure 2. Furthermore, a gap height of 6 μm is interpreted as the threshold before the mixed friction occurs from asperity contact between the rough surfaces. Therefore, the analysis is terminated at this threshold.

3.4.1. Step-size constraints

The step-size is variable in order to reduce the required computation effort. However, movement of solid walls require dynamic changes in the surrounding mesh, why it is necessary to constrain the step-size. Furthermore, rapid deceleration will occur when nearing the seat and if this effect is to be captured, a sufficiently small step-size is necessary. This is the reason for creating a UDF, which continuously updates the maximum allowed step-size.

If the distance displaced by the plunger in one time-step is above the mesh element length, the mesh update will fail. This means that the step-size must always be constrained to consider this, while still allowing finding a solution rapidly. The total allowed displaced distance is:

$$\Delta S = 2\tau_{max}\dot{z} \rightarrow \tau_{max} = \frac{\Delta S}{2|\dot{z}| + \varepsilon} \quad (6)$$

where ε is a small number to avoid singular values. The allowed distance (ΔS) is half of the maximum distance moved by the plunger in one step, and is defined as a linear function that depends on the valve lift. The information about maximum and minimum cell size from Table 1 is used to define the gradient:

$$\Delta S = \frac{S_e - S_s}{l_s} z + S_s \quad (7)$$

The upper and lower level are directly correlated to the maximum (S_e) and minimum (S_s) element height in Zone 2. This prevents steps that results in negative

mesh volumes, while making approximation of the end damping forces possible.

4. Simulation cases with results

The presented numerical methodology can be applied to most seat type valves. The features of a given design can then be evaluated by defining boundary conditions and the dynamic behaviour of the plunger. The features of interest are based on gaps in the state of the art, especially regarding flow and force dependencies on plunger, lift and velocity. This results in the two boundary condition cases:

- *Case A*: Active valve closing with either constant velocity or acceleration where $p_1 - p_2 = \Delta p = 0$ bar
- *Case B*: Active valve closing with variable acceleration $\Delta p = 0.1$ bar

Each case represents a theoretically possible situation, though practically tedious. This benefit of simulation allows extracting information that is relevant when trying to simplify the CFD framework into a LPM. The computational effort of a LPM is substantially lower than CFD, which is desired for design frameworks. A simulation example of *Case B* is presented in Figure 3. The figure shows that the fluid velocity increases under the plunger and maintains this higher velocity when moving down the annular outlet. The jet angle varies with lift and the jet velocity is also observed to increase with a decrease in lift.

4.1. Active valve closing with $\Delta p = 0$ bar

The consequences of a moving member through the fluid were analysed by simulating an initially stationary fluid and plunger. The plunger moves through

the medium with different velocities. This describes how the fluid moves around the plunger and is useful to determine the movement-induced flow and forces acting on the plunger. One simulation is carried out with three different mesh refinements (to show grid-independence) and the results of this give a relative error, which is well below the numerical uncertainty (the force deviates most by 2%).

The flow solely caused by plunger movement (movement-induced flow) and the mass of this displaced fluid relates to the mass added by the fluid to the plunger (i.e. the ‘added mass’ of a sphere is equal to half of the displaced mass (Brennen 1982)). The relation between the two varies with geometry, but should according to this be directly proportional. The regular approach is to multiply plunger velocity with its shadow area (in this case equal to $5e-4$ m²). This is investigated by computing the displaced fluid at various velocities and accelerations. The movement-induced flow is divided by the plunger velocity to reveal the effective plunger area (A_{fp}). The results are shown in Figure 4.

It is observed from Figure 4(a) that A_{fp} is both varying with position and velocity (i.e. modelling the flow caused by plunger movement by a constant area times the plunger velocity is erroneous, at least for this design). Figure 4(c) shows a correspondence between A_{fp} dependency on plunger lift, while the acceleration is constant and non-zero (realistic switching case). In conclusion, A_{fp} does match the final value of the plunger’s shadow area, but only near the seat, thus a power law function may serve as a better representation.

In Figure 4(b) and (c) there is a clear difference in the forces near full valve opening ($z = 2.5$ mm). The main difference of the two forces is that the simulation with constant velocity will have $\dot{z} = 0$ at $t < 0$, but when $t > 0$ the velocity will instantaneously build-up to $\dot{z} = \dot{z}_0$, where \dot{z}_0 is the value of the instantaneous

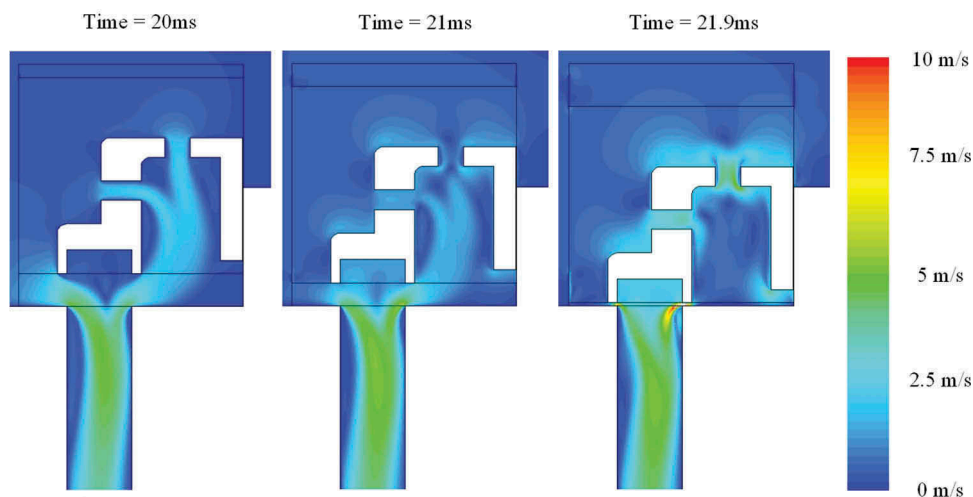


Figure 3. Example of CFD computations showing the fluid domain velocities at three time instances of a *Case B* simulation. The switching is initiated at 20 ms when the flow is fully developed and upon nearing the seat, the fluid velocity exceeds 10 m/s. Computation time: 1 h.

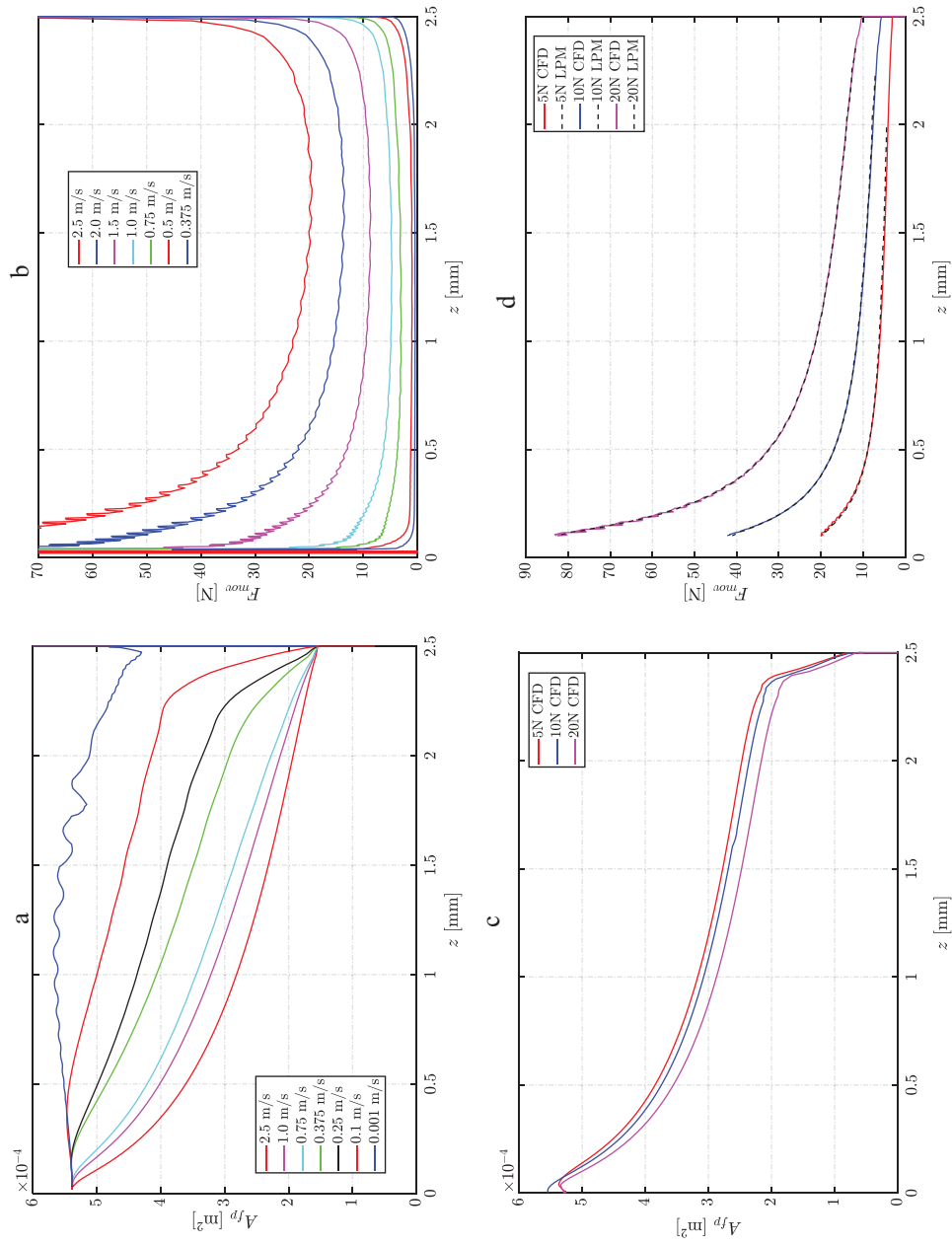


Figure 4. CFD results corresponding to Case B: showing the transient plunger displaced flow area (A_{fp}) and fluid force as function of plunger lift (z). The force predicted from the lumped parameter model (LPM) is shown with a black dotted line in (d) This model is described later in Section 5.

constant velocity. That is, an infinite acceleration is experienced at $t = 0$. The time-integration of this is finite and this impulsive drag on a sphere moving in an unbounded fluid domain is shown to be proportional to \dot{z}_0 . The general expression for the impulsive drag force on a sphere is (Landau and Lifshitz 1956):

$$\begin{aligned} F_{v,sphere} &= 6\pi\rho\nu R\dot{z}_0 \left(1 + \frac{R}{\sqrt{\pi\nu t}}\right) + \frac{2}{3}\pi\rho R^3\dot{z}_0\delta(t) \\ &= \left(k_v + \frac{k_{I,d}}{\sqrt{t}}\right)\dot{z}_0 \end{aligned} \quad (8)$$

where R is the radius of the sphere, ν the kinematic viscosity and $\delta(t)$ is Dirac's delta function. The time (t) is seen to monotonically decrease the impact drag until this transient term becomes insignificant and the expression reduces to the form, $k_v\dot{z}$. The values and dependencies of these coefficients can be approximated from the CFD framework, and the results are shown in Section 5.

4.2. Active valve closing with $\Delta p = 0.1$ bar

The movement-induced flow and forces have been identified. Therefore, this case combines a valve switching

with a constant pressure differential of 0.1 bar maintained by the pressure boundaries of Zone 1 & 5. This is done to reveal the transient flow and force response, and the results of this analysis are presented in Figure 5.

Figure 5 shows that it takes around 20 ms for the flow to fully develop, at exactly 20 ms the valve is actuated by 80 N and the plunger moves according to Equation (5) towards the seat. The movement-induced flow creates a 'bump' on the flow profile before it goes to zero upon reaching the seat. The figure shows a discrepancy between the two models while switching. The flow of the LPM changes more rapidly to zero, which will affect the flow forces; however, the modelling of these transient flow forces is within an acceptable error margin. In conclusion, this means that either fluid inertia or movement-induced flow is too simplified.

The fluid force in Figure 5 initially follows the proposed modified flow force model. At 20 ms the movement-induced force starts to play a role and while the valve is closing the flow force changes accordingly which attenuates the high damping. The results of the CFD compared to the LPM show sufficient coherence and the description of these forces and remaining LPM are given in the following section.

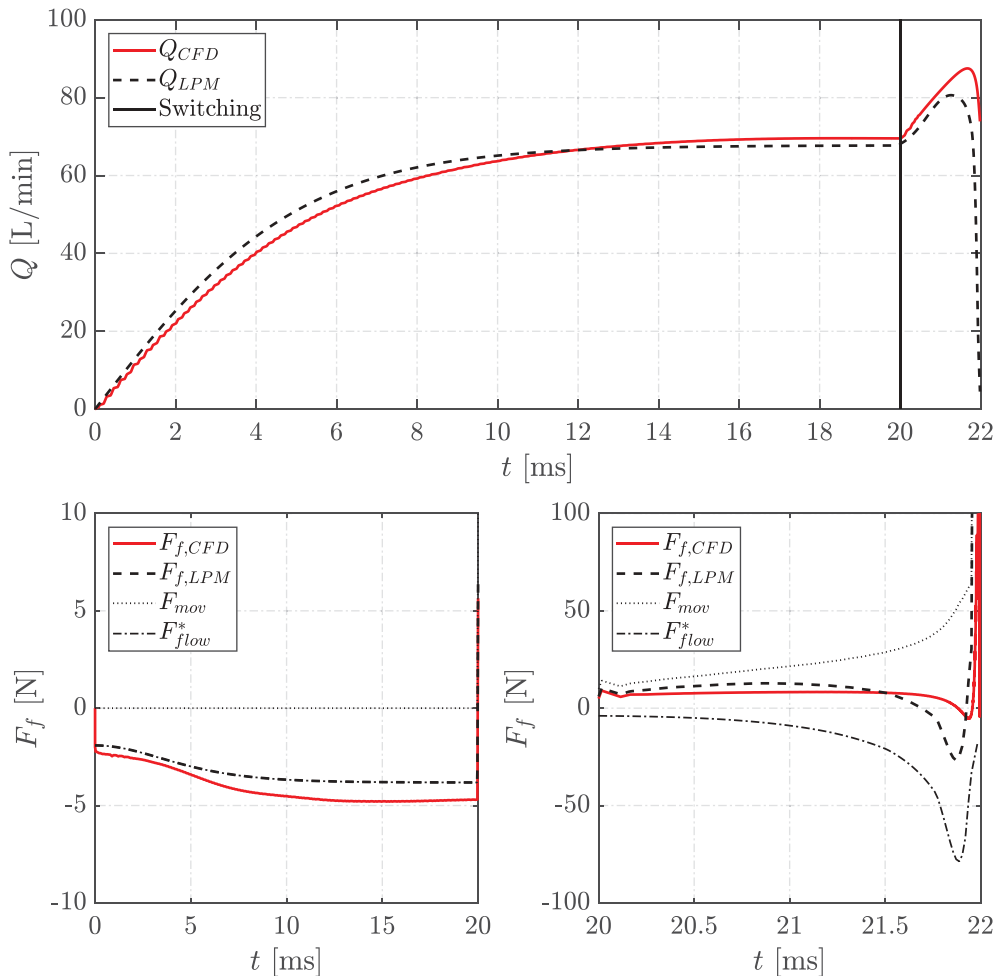


Figure 5. Case C: Comparison of CFD and LPM flow and forces. Switching is initiated at 20 ms and $\Delta p = 0.1$ bar. The force graph is split into two different time-frames to better illustrate the switching period.

5. LPM

As previously mentioned, some engineering tasks only require a lumped model, and the required level of accuracy varies. The governing equations of such a methodology based on the relations found by CFD are presented here.

A closed valve does not conduct flow and its fluid force is proportional to pressure differential. When open, the fluid force will consist of a contribution from the flow and the movement of the plunger. The fluid force is defined as:

$$F_f = \begin{cases} F_{flow}^* - F_{mov} & \text{if } z > z_{min} \\ -A_{fp}\Delta p & \text{else} \end{cases} \quad (9)$$

where z_{min} is the minimum lift corresponding to surface roughness (6 μm), which prevents computation of singular values. The force F_{flow}^* is a result of the conducting flow in the valve seat, F_{mov} is the force induced by plunger movement and A_{fp} is the shadow area where the pressure differential acts when the valve is not conducting flow.

5.1. Movement-induced force

The movement-induced force acting from the fluid on the plunger plays a role in the plunger dynamics. For a plunger with design as presented in this article this force has been proposed to follow the expression describing Stokes-flow drag with an additional Drag term (Lai and Mockros 1972):

$$F_{mov} = \underbrace{k_a \ddot{z}}_{\text{Added mass}} + \underbrace{k_v \dot{z}}_{\text{Viscous}} + \underbrace{k_d \dot{z}|\dot{z}|}_{\text{Drag}} + \underbrace{k_h \int_0^t \frac{dz}{\sqrt{t-\tau}} d\tau}_{\text{History}} \quad (10)$$

where k_a is the virtual mass of accelerated fluid, k_d is the drag coefficient, k_v is the viscous shearing coefficient, k_h is the history coefficient and τ is a step-size where the assumption of piecewise constant acceleration is valid. One procedure to determine the coefficients was shown in Bender *et al.* 2017a, where experimental validation showed that the history term is not significant for the overall dynamics. Furthermore, a position dependency of k_a , k_v , k_d was revealed. The study did not cover possible non-linearities when changing the velocity. Therefore, simulations with different constant velocities has been performed to determine $k_{I,d}$, k_v and k_d . It should be noted that $k_{I,d}$ is only used to describe the impulsive drag to allow accurate representation of k_v . This is used to check the validity of Equation (10). If the coefficients are in fact velocity independent, the results will reveal equal values for the coefficients. The results are shown in Figure 6.

Figure 6 shows that the viscous coefficient determined by simulation is velocity independent, since one order of magnitude difference does not change the value noticeably. On the contrary, the values of k_d showed discrepancies when changing the velocity. Therefore, the drag coefficient has been plotted as function of lift and velocity. If the knowledge about hydrodynamic damping of a design is critical, it is necessary to study this effect.

By applying the data from the constant acceleration tests in Figure 4(c) (where also the force predicted by the LPM is depicted), the added mass coefficient can be determined and thereby the force can be predicted. Figure 4(c) reveals a nice coherence between CFD and LPM and is comparable to the results obtained from a full 3D CFD analysis (Roemer *et al.* 2015b). The added mass (k_a) is seen in Figure 6(c).

Ideally, the three plots should lay on top of each other, but a variation of 2 g at worst case exists, by either numerical uncertainties or erroneous LPM structure. The mass of the plunger ranges from 19–30 g, which means the error is at maximum 10%.

5.2. Flow force

The flow forces acting on a poppet valve is normally derived from the change in momentum of the fluid entering and leaving a control volume (Bernoulli force). This constitutes a static term that is proportional to the square of the flow rate. Furthermore, when the fluid inside a control volume accelerates (i.e. change in flow rate), this also causes a change in momentum that is proportional to the derivative of the flow rate. This gives the expression:

$$F_{flow} = -\rho(l_d \dot{Q} + \bar{u}Q) \quad (11)$$

where l_d is the damping length which is approximately equal to the hydraulic diameter (for annular seat valve that is $2z$), \bar{u} is the mean velocity of fluid near the flow edges approximated by:

$$\bar{u} = \frac{|Q|}{C_d A_o}; \quad A_o = 2\pi(2(r_1 + l) + w)z \quad (12)$$

where C_d is the discharge coefficient used to describe the ‘actual’ flow area by scaling the opening area of the valve (A_o), and the area is defined by the parameters seen in Figure 1. An experimental study of the steady-state flow forces in the annular seat valve of this research was presented in (Noergaard *et al.* 2017a). The data of the flow forces showed to fit a model utilising the plunger shadow area (A_{fp}) multiplied with the pressure differential, which works well when the valve lift is low. However, when the valve stroke is changed and the flow direction is switched this model is not accurate. This is

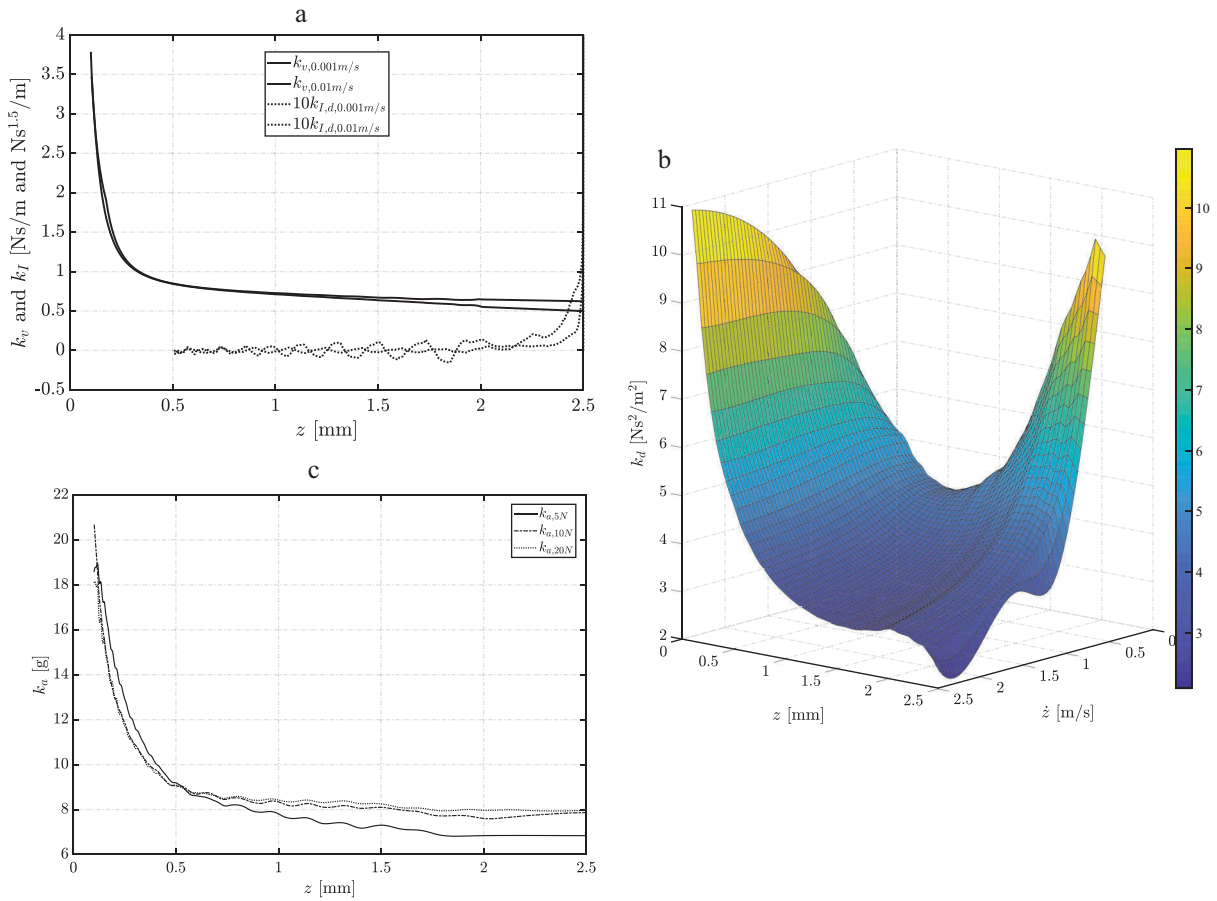


Figure 6. CFD results corresponding to *Case B* have been used to determine the lumped parameters shown here. Low velocities are used for (a) since this causes the drag term to be insignificant. Then the drag coefficient can be determined as shown in (b) and finally the added mass of (c). Near end-stop the solution of pressure starts to oscillate resulting in the observed scattering of k_a .

demonstrated in [Figure 7](#) where CFD analysis is used to compute steady flow forces and the pressure differential as a result of 120 l/min flowing through the valve. These CFD results have been used to rewrite the flow force model into:

$$F_{flow}^* = \begin{cases} (2F_{flow} - A_{fp}\Delta p) \cos \left(\underbrace{\tan^{-1} \left(\frac{11z^2}{w^2} \right)}_{\gamma_+} \right) & \text{if } \Delta p > 0 \\ (F_{flow} - A_{fp}\Delta p) \cos \left(\underbrace{1.22 \tan^{-1} \left(\frac{z}{w} \right)}_{\gamma_-} \right) & \text{else} \end{cases} \quad (13)$$

This model is based on known physical quantities but with ‘empirical correction factors. The structure of the LPM is similar to classical flow force models for poppet type valve where a jet angle (γ) determines how much of the flow force is acting in the closing direction. The results of this model compared with the traditional steady-state model are demonstrated in [Figure 7](#).

The figure shows how the classic steady-state model (F_{flow}) lacks accuracy when the lift gets below 1 mm, but this is remedied by the proposed modifications.

Furthermore, the force and pressure changes characteristic with flow direction, which is now also approximated. However, during negative pressure differential the LPM does not encapsulate the hard non-linearity that occurs above 10 mm. This is though insignificant, since the magnitude of the flow force is below 1 N at this instant. This new LPM thus explains how the valve will behave in a wide range of valve lifts. Potentially enabling designs where nearly no flow force acts on the plunger.

5.2.1 Orifice flow

The transient flow profile as predicted by the incompressible and viscous CFD analysis is depicted in [Figure 5](#) and the result indicate that a quasi-static form is not accurate. This flow gradient can be described by Euler’s equation of momentum (unsteady potential flow), which is derived for an orifice in ([Funk et al. 1972](#)). The simple form of the flow gradient is:

$$\dot{Q} = \frac{\Delta p - \Delta p_{QS}}{k_{\dot{Q}}} \quad (14)$$

where Δp is the pressure difference of the boundary conditions, Δp_{QS} is the quasi-steady pressure drop and $k_{\dot{Q}}$ is the fluid-inductance. For an orifice this is ([Funk et al. 1972](#)):

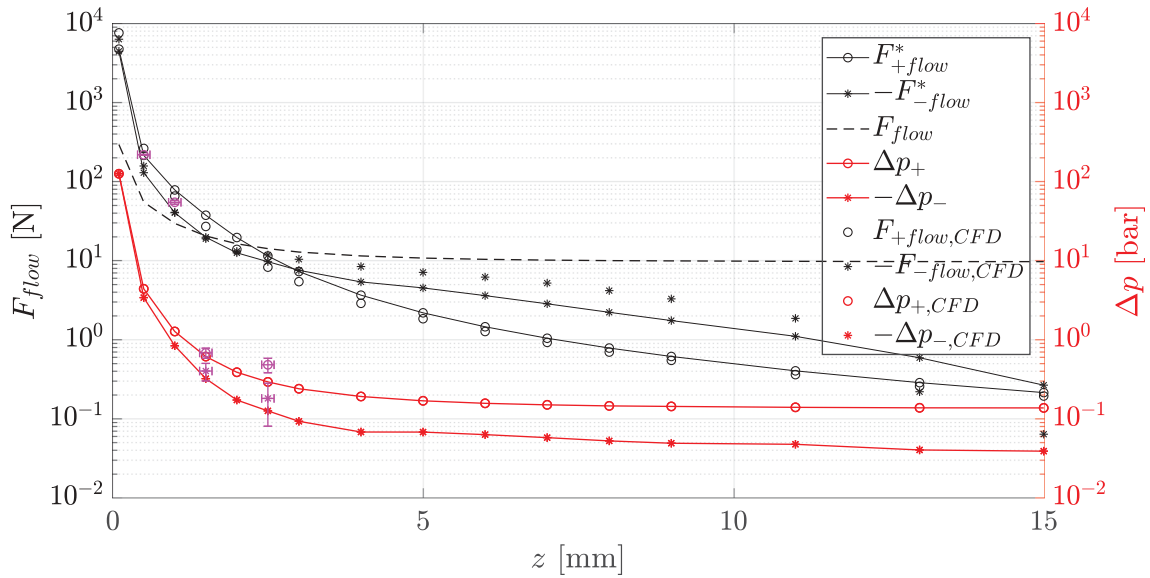


Figure 7. Flow force evaluation and pressure differential from CFD and LPM simulations. The magenta coloured dots indicate experimental values from (Noergaard *et al.* 2017a) and the ranges indicate uncertainty. The LPM model results are drawn with lines and the raw CFD data is illustrated without lines. The '+' and '-' indicate either positive or negative Δp .

$$k_{\dot{Q}} = \frac{\rho}{\sqrt{0.5\pi C_d A_o}} \quad (15)$$

The quasi-steady pressure drop (Δp_{QS}) may be represented by the orifice equation with or without modifications to account for laminar flow. The CFD analysis has shown that flow from the plunger takes the form: $Q_{plunger} = A_{fp}\dot{z}$. Therefore, the classical orifice equation is combined with this expression to yield:

$$\begin{aligned} Q &= Q_{QS} - Q_{plunger} \\ &= C_d A_o \sqrt{\frac{2}{\rho} \sqrt{|\Delta p_{QS}|} \text{sign}(\Delta p_{QS})} - A_{fp}\dot{z} \end{aligned} \quad (16)$$

$$\Delta p_{QS} = (Q + A_{fp}\dot{z}) \left| Q + A_{fp}\dot{z} \right| \underbrace{\frac{\rho}{2(C_d A_o)^2}}_{k_f} \quad (17)$$

Equation (17) can be inserted into Equation (14) and solved which leads to the flow shown by the dashed line in Figure 5. The overall characteristics are sufficient for the entire simulation except near the end-stop where the flow from the LPM is lower than it should be. In total, the LPM does capture the overall characteristics with some inaccuracies. Note that as $k_{\dot{Q}}$ goes to zero (decrease of A_o) the pressure gradient goes to infinity. This results in the transient effect becoming obsolete and the flow takes the classical quasi-steady form.

6. Conclusion and outlook

The main features of an ACV have been investigated when operating with an incompressible piezo-viscous VG-46 oil. A numerical framework established exactly with the purpose of analysing a valve of this type was used. This framework allowed simulation of

dynamic switching of the valve, as well as simulation of flow and forces acting on the plunger.

The application of the developed CFD framework revealed novel forms of LPM compared to the ones previously applied in digital hydraulics (Roemer *et al.* 2014, 2015a, Knutson and Van De Ven 2016, Bender *et al.* 2017a). The differences concern fluid displaced by the plunger (until now been considered a constant area times velocity), flow inductance (so far modelled as quasi-static) and the drag coefficient (k_d) now both plunger lift and velocity dependent (until now just a constant, or lift dependent). All these phenomena may potentially be relevant to consider in a design framework, but the exact impact is yet to be investigated. The simulations show a large hydrodynamic damping force and an almost equal flow force in opposite direction at end-stop of the ACV, which is useful knowledge when designing valves with regards to durability. In total it was shown by CFD simulation, that the process of establishing LPMs is not trivial.

Future work concerns design of a test-rig for validation of the movement-induced fluid force and flow. The confidence that the framework is accurate is important when used for design purposes. Furthermore, the presented LPM will be relevant to apply in a design optimisation to visualise its influence.

Disclosure statement

No potential conflict of interest was reported by the authors.

Funding

This work is funded by the Danish Council for Strategic Research via the HyDrive-project (case no. 1305-00038B). The authors are grateful for the funding.

Notes on contributors

Niels Christian Bender received his B.Sc. and M.Sc. degrees in mechatronic control engineering from Aalborg University, Aalborg, Denmark, in 2014 and 2016 respectively. Since 2016 he has been a Ph.D. fellow at the Department of Energy Technology, Aalborg University, with a research focus on design of digital hydraulic on/off valves.


Henrik Clemmensen Pedersen has been Associate Professor at the Department of Energy Technology, Aalborg University, Aalborg, Denmark, since 2009 before becoming Professor at the same department in 2016. His research interests include analysis, design, optimisation, and control of mechatronic systems and components, with special focus on fluid power systems for wind and wave energy applications. He is an author of more than 100 papers in international journals and conferences.

Bernd Winkler obtained his Bachelor's degree in Mechatronics in 2000 and doctoral degrees in 2004 both from the Johannes Kepler University in Linz, Austria. He has been an employee of Linz Center for Mechatronics (LCM) GmbH since 2005. Currently he serves as the Business Unit Manager and head of Advanced Hydraulic Drive in LCM GmbH.

Andreas Plöckinger obtained his Bachelor's degree in Mechatronics in 2001 from the Johannes Kepler University in Linz, Austria. He has been an employee of Linz Center for Mechatronics (LCM) GmbH since 2002. Currently he serves as a Senior Researcher in LCM GmbH focusing on integrated electro-hydraulic hybrid drives.

ORCID

Niels Christian Bender  <http://orcid.org/0000-0002-1543-0244>

Henrik Clemmensen Pedersen  <http://orcid.org/0000-0002-1034-3280>

References

Bardina, J.E., Huang, P.G., and Coakley, T.J., 1997. Turbulence Modeling Validation, Testing, and Development. *Technical report, NASA Technical Memorandum, Ames*.

Bender, N.C., et al., 2017b. Towards a modelling framework for designing active check valves a review of state-of-the-art. *International Journal Fluid Power*, 19 (01), 49–64. doi:10.1080/14399776.2017.1377027

Bender, N.C., Pedersen, H.C., and Nørgård, C., 2017a. Experimental Validation of Flow Force Models for Fast Switching Valves. *Proceedings ASME Symposium Fluid Power Motion Control* (Sarasota).

Brennen, C.E., 1982. A Review of Added Mass and Fluid Inertial Forces. *Technical Report January, Naval Civil Engineering Laboratory, California*.

Ehsan, M., Rampen, W.H.S., and Salter, S.H., 2000. Modeling of digital-displacement pump-motors and their application as hydraulic drives for nonuniform loads. *Journal Dynamics Systems Measurement Control*, 122 (1), 210–215. doi:10.1115/1.482444

Funk, J.E., Wood, D.J., and Chao, S.P., 1972. The transient response of orifices and very short lines. *Journal Basic Engineering*, 94 (2), 483–489. doi:10.1115/1.3425456

Hansen, R.H., Kramer, M.M., and Vidal, E., 2013. Discrete displacement hydraulic power take-off system for the wavestar wave energy converter. *Energies*, 6 (8), 4001–4044. doi:10.3390/en6084001

Huova, M., Laamanen, A., and Linjama, M., 2010. Energy efficiency of three-chamber cylinder with digital valve system. *International Journal Fluid Power*, 11 (3), 15–22. doi:10.1080/14399776.2010.10781011

Knutson, A.L. and Van De Ven, J.D., 2016. Modelling and experimental validation of the displacement of a check valve in a hydraulic piston pump. *International Journal Fluid Power*, 17 (2), 114–124. doi:10.1080/14399776.2016.1160718

Kogler, H., et al., 2010. A Compact Hydraulic Switching Converter for Robotic Applications. In *Proc. ASME Symp. Fluid Power Motion Control*, 56–68, Bath.

Lai, R.Y.S., 1973. Translatory Accelerating Motion of a Circular Disk in a Viscous. *Fluid Applications Sciences Researcher*, 27 (1), 440–450. doi:10.1007/BF00382506

Lai, R.Y.S. and Mockros, L.F., 1972. The Stokes-flow drag on prolate and oblate spheroids during axial translator accelerations. *Journal Fluid Mechanisms*, 52 (1), 1–15. doi:10.1017/S0022112072002939

Landau, L.D. and Lifshitz, E.M., 1956. *Fluid mechanics. Elsevier, second edition*.

Lewis, R., 2007. A modelling technique for predicting compound impact wear. *Wear*, 262 (11–12), 1516–1521. doi:10.1016/j.wear.2007.01.032

Malalasekera, W. and Versteeg, H.K. 2006. *An Introduction to Computational Fluid Dynamics - The Finite Volume Method*. Vol. 44. US:Pearson Education.

Noergaard, C., et al., 2015. Experimental Validation of Modelled Fluid Forces in Fast Switching Hydraulic On/Off Valves. *Int Conf Fluid Power Mechatronics*. pages 68–73. China: IEEE.

Noergaard, C., et al., 2016. Optimization of Moving Coil Actuators for Digital Displacement Machines. In: *Eight Work. Digit. Fluid Power*. Tampere, Finland: Tampere University of Technology.

Noergaard, C., 2017. Design, Optimization and Testing of Valves for Digital Displacement Machines. *Phd dissertation*, Aalborg University.

Noergaard, C., et al., 2017. *Test-rig for Valves of Digital Displacement Machines*. In *Ninth Work. Digit. Fluid Power*. Aalborg: Aalborg University, 1–13.

Noergaard, C., et al., 2017a. Flow Characteristics and Sizing of Annular Seat Valves for Digital Displacement Machines. *Modeling, Identification and Control*, 31 (1), 1–13.

Roemer, D.B., et al., 2013. Method for Lumped Parameter Simulation of Digital Displacement Pumps/Motors Based on CFD. *Applications Mechanisms Materials*, 397–400, 615–620. doi:10.4028/www.scientific.net/AMM.397-400.615

Roemer, D.B., et al., 2014. Optimum design of seat region in valves suitable for digital displacement machines. *International Journal Mechatronics Autom*, 4 (2), 116–126. doi:10.1504/IJMA.2014.062339

Roemer, D.B., et al., 2015a. Optimum design of a moving coil actuator for fast switching valves in digital hydraulic pumps and motors. *IEEE/ASME Trans. Mechatronics*, 20 (6), 2761–2770. doi:10.1109/TMECH.2015.2410994

Roemer, D.B., Pedersen, H.C., and Andersen, T.O., 2015b. Modeling of Dynamic Fluid Forces in Fast Switching

- Valves. In *Proc. ASME Symp. Fluid Power Motion Control*, 1–10, Chicago.
- Uusitalo, J.P., *et al.*, 2010. Novel bistable hammer valve for digital hydraulics. *International Journal Fluid Power*, 11 (3), 35–44. doi:[10.1080/14399776.2010.10781013](https://doi.org/10.1080/14399776.2010.10781013)
- Wilfong, G., Bardorff, M., and Lumkes, J., 2011. Design and analysis of pilot operated high speed on/off valves for digital pump/motors. *Proc. 52nd Natl. Conf. Fluid Power*. National Fluid Power Association, pages 259–269.
- Winkler, B., Plöckinger, A., and Scheidl, R., 2010. A novel piloted fast switching multi poppet valve. *International Journal Fluid Power*, 11 (3), 7–14. doi:[10.1080/14399776.2010.10781010](https://doi.org/10.1080/14399776.2010.10781010)